CrystEngComm

Accepted Manuscript

ROYAL SOCIETY OF CHEMISTRY

www.rsc.org/crystengcomm

Plasma assisted synthesis and high pressure studies of structural and elastic properties of metal nitrides XN (X=Sc,Y)

Ridong Cong[a], Xiaoyu Liu[b], Hang Cui[a], Jian Zhang[a], Xiaoxin Wu[a], Qiushi Wang[a], Hongyang Zhu[a]*, and Qiliang Cui[a]

[a] State Key Laboratory of Superhard Materials, Jilin University, Changchun 130012, People's Republic of China

[b] College of Physics, Jilin University, Changchun 130012, People's Republic of China

* To whom correspondence should be addressed.

E-mail: hongyangzhu@jlu.edu.cn, Phone: 86-431-85168346, Fax: 86-431-85168346.

Abstract

ScN and YN crystals were synthesized through direct nitridation of metal with nitrogen using plasma assisted direct current arc discharge method. Structural characterization indicates that the as-synthesized ScN crystals are single crystalline and YN crystals are polycrystalline with grain sizes range from 5-15 nm. High pressure structural and elastic properties of ScN and YN crystals were carried out using angle dispersive synchrotron radiation in a diamond anvil cell up to 53.9 and 53.5 GPa, respectively. No phase transition occurred in the pressure ranges we achieved in this study, which is in accord with the theoretical studies that ScN and YN are stable under high pressure. The measured zero-pressure bulk modulus for ScN coincides with those of theoretical results while YN yield a bulk modulus much higher than the theoretical values exhibiting reduced compressibility. It is considered to be caused by the decreased grain sizes in the characteristic polycrystalline YN.

Keywords: Arc discharge, High-pressure behaviors, X-ray diffraction, Crystal structure, Compressibility,

1. Introduction

Recently, there has been extensive interest in scientific and technological application of transition metal nitrides (TMNs) amongst which ScN and YN in particular turned out to be very promising due to their unique physical properties of high hardness, mechanical strength, high temperature stability, and outstanding electronic transport properties related to their well-known rocksalt structure type (B1).[1-4] In addition, ScN and YN are particularly intriguing because they are the few TMNs that are also semiconductors.[5-7] ScN is also an ideal buffer layer or substrate for the growth of high quality GaN crystals, GaN/ScN heterostructures, or ScGaN alloys due to their small lattice mismatch.[8-10] Similarly, incorporation of ScN and YN into other compound nitrides systems such as $Y_xAl_yGa_{1-x-y}N$ alloys,[11] $Sc_{1-x}Ti_xN$ layers,[12] YN/ScN,[13] ZrN/ScN and HfN/ScN superlattice[14, 15] are expected to have promising applications in future photoelectric and thermoelectric devices. Moreover, ScN and YN may also act as hosts for magnetic transition metals as indicated by recent theoretical studies.[16, 17]

In the past decades, much attention has been paid to the growth of ScN and YN films with different orientations and levels of epitaxial on different substrates through the control of processing condition.[2, 4, 7, 18-20] All of these methods, conventionally, foreign substrates are always needed for the growth of epitaxial films, as a result, the structural defects such as dislocation and residual stress caused by the lattice mismatch between films and substrates, which affect the crystal quality of the obtaining films and then limit their further applications.[7, 18] Different from the film structures, bulk crystals endure much lower dislocation densities than in thin films on foreign substrates. In spite of that, only a few studies reported the synthesis of ScN and YN crystals. In the early 20th century, researchers obtained ScN and YN powders using direct reaction of metal with nitrogen gas, ammonia, or metal hydrides with ammonia at high temperatures.[21-24] Unfortunately, the kinetics of the reaction of Sc with nitrogen or ammonia is slow and may result in nitrogen deficient product with bulk compositions depending on *T*.[24] Early

attempts to prepare ScN also included the reaction of Sc_2O_3 with carbon in nitrogen atmosphere, but the products contained significant amounts of oxygen and/or carbon.[25] In recently years, Niewa *et al.*[26] introduced three different ways including the direct nitridation of Sc metal, decomposition of $Li_3[ScN_2]$, and nitridation of intermetallic Sc-In phase, which leaded to high quality single ScN samples with low oxygen content in a broad range of particle sizes such as fine powders with particle sizes smaller than 200 nm and single crystals of up to 1 mm. Further studies by Zheng[27] and Li[28] showed that ScN and YN bulk crystals can be grown on tungsten foil under a nitrogen atmosphere using sublimation-recondensation method, in which the influence of temperature and pressure on crystal growth was investigated. These approaches, however, normally require complex procedures, substrate, and long reaction times. In some cases, sophisticated and expensive heating systems and significant amounts of energy are required to maintain the high temperature conditions for long periods of time. These drawbacks limit the efficiency of synthesizing materials using these methods. Therefore, one of the purposes of this work is to explore a rapid, low cost and high yield of method for synthesizing ScN and YN bulk crystals.

To provide a basis for understanding future device concepts and applications, knowledge of the fundamental properties of the devices is required. For example, information on the pressure dependence of these properties is very important for the application. As a matter of fact, pressure tuning studies of many physical properties as a function of volume have proved invaluable in systems ranging from the electronic structure of semiconductors to photo-physics of solid state molecular structures.[29] In spite of the prospective applications of ScN and YN, only limited theoretical studies have been reported on their physical properties under high pressure. Recent research outcomes from synchrotron radiation and powder X-ray diffraction demonstrated that under high pressure the majority of binary compounds with NaCl (B1) structure undergo a phase transition to the CsCl (B2) structure.[30] Up to now, the phase transition from B1 to B2

have been predicted at transition pressures of 333-364 GPa for ScN[3, 31-33] and 136-138 GPa for YN[34, 35] separately, depending on the applied theoretical methods. Moreover, the possibility of two phase transitions for ScN from the NaCl (B1) to the orthorhombic CaSi (Cmmc) structure above 252 GPa and to the tetragonal AuCu (P4/mmm) structure at 303 GPa have also been reported.[36] The corresponding calculated bulk moduli of ScN and YN range between 201-222 GPa[3, 6, 37, 38] and 154-163 GPa[6, 34, 35], respectively. However, no experimental data confirming any of the theoretical predictions have been obtained so far, the information regarding the stability of crystal structure, pressure dependence of cell volume as well as the elastic properties is still lacking.

In this paper, we demonstrate potentially a novel but simple and efficient method of synthesizing ScN and YN crystals, in which the direct nitridation of Sc and Y metals in plasma-assisted direct current (DC) arc discharge with N_2 as the working medium. This technique is attractive for its ability to produce bulk crystals with growth rate orders of magnitude higher than thin films. Furthermore, the as-prepared ScN and YN have been further investigated by means of in situ X-ray diffraction to explore the structural and elastic properties of these nitrides under high pressure.

2. Experimental Section

Synthesis of ScN and YN bulk crystals. The synthesis was carried out in an improved DC arc discharge plasma setup.[39] Both ScN and YN were synthesized following the same process. A tungsten rod with the purity higher than 99.99%, 5 mm in diameter and 30 cm in length was used as the cathode. Rare metal (Sc, Y) (purity 99.99%) and N_2 gas (purity 99.999%) were used as sources, respectively. The ingot metal was placed into a water-cooled graphite crucible which acted as the anode. The reaction chamber was evacuated to less than 1 Pa then filled with N_2 several times to remove residual air completely. Then the working gas (N_2, purity: 99.999%) was introduced into the chamber until the inner pressure reached 40 kPa, which provided an excess nitrogen pressure for the fully nitridation of the metals. The input current was maintained at 100 A, and the

voltage was a little higher than 20 V. The power supply was turned off 15 min later. After passivation in Ar for 5h, the metallic gray or blue-green fragile coarse powders were collected at the anode.

Characterization. Structural analysis of the products was carried out by powder X-ray diffractometry (XRD) on a Rigaku D/max γA diffractometer using Cu Kα radiation (λ= 0.154178 nm). Scanning electron microscope (SEM) images of the sample were taken on a HITACHI S4800 microscope equipped with an energy-dispersive X-ray spectroscopy (EDS). High resolution transmission electron microscope (HRTEM) images and the selected area electron diffraction (SAED) patterns were obtained via a JEM-2200FS transmission electron microscope using an accelerating voltage of 200 kV. The pressure was generated in a diamond anvil cell (DAC) with 300 μm culet diamond anvils. A 70 μm diameter hole was drilled through the center of a T-301 stainless-steel gasket to form a sample chamber. The samples with a tiny ruby chip were placed inside the sample chamber and filled with quasi-hydrostatic pressure medium (methanol/ethanol 4:1). The in situ high-pressure X-ray diffraction measurements were performed with angle-dispersive synchrotron X-ray source (0.4066 Å) at beamline X17C of National Synchrotron Light Source, Brookhaven National Laboratory. The Bragg diffraction rings were recorded with a MAR165 CCD detector, and the XRD patterns were integrated from the images with FIT2D software.

3. Results and Discussion

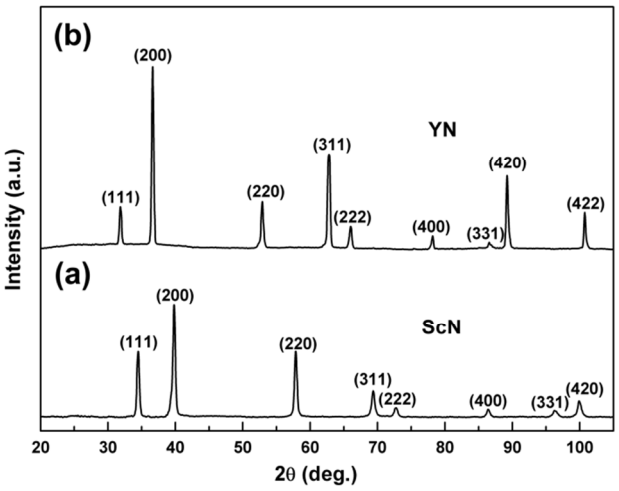

Figure 1. Typical XRD patterns of the as-prepared samples. (a) ScN and (b) YN.

Figure 1 displays the typical XRD patterns of the as-synthesized samples. As shown in Figure 1a, eight clear and sharp peaks can be distinguished from the pattern, and by using the Reflex module combined in the Materials Studio program (Accelrys Software Inc.), all the observed peaks can be unambiguously indexed as the (111), (200), (220), (311), (222), (400), (331), (420) diffractions of face-centered cubic lattice of ScN with the cell parameters a=4.498 Å, V_0=91.01 Å^3. Figure 1b shows the XRD pattern of YN which exhibits the same lattice structure as ScN, the cell parameters are a=4.894 Å, V_0=117.21 Å^3. These results are in good agreement with the known values of rocksalt (NaCl) structure (space group: Fm3m (225)) of ScN (JCPDS file No. 45-0978) and YN (JCPDS file No. 35-0779). No peaks of any other phases or impurities can be found in the XRD patterns.

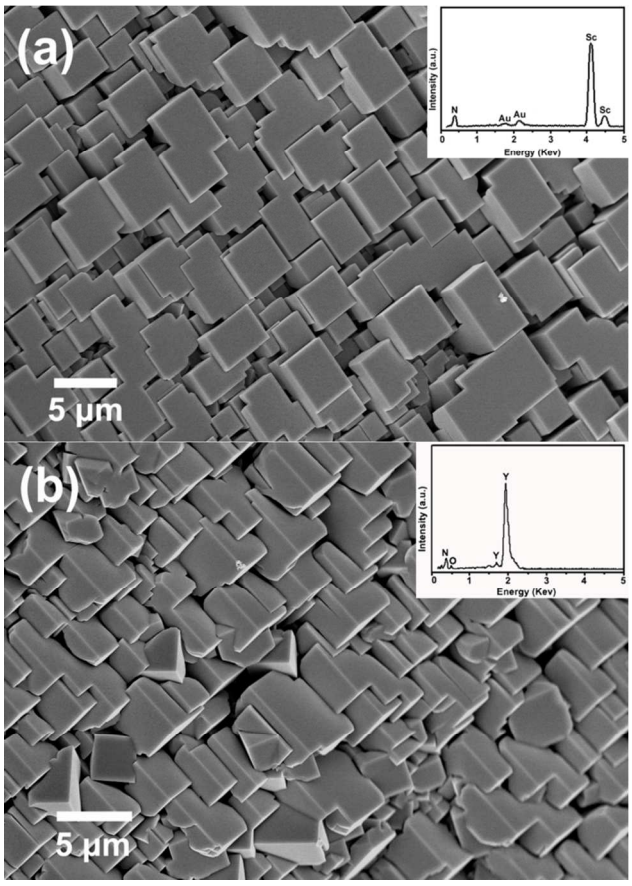

Figure 2. SEM images of the as-prepared ScN (a) and YN (b). The insets are their corresponding EDS images.

Figure 2 displays the SEM images of the as-prepared samples. As shown in Figure 2a, the ScN crystals are square, rectangular in morphology/shape with smooth surfaces. Some of the crystals tend to merge together along the grains boundaries and the average dimensions of these crystals are 5 μm. EDS analysis (inset on the right-up corner in Figure 2a) shows that ScN crystals are composed of scandium and nitrogen with the atomic ratio of N:Sc to be about 1:1.03, indicating a slightly excessive Sc. Figure 2b is the SEM image of the as-prepared YN crystals which are still close to cuboidal in general shape and the sizes are similar to those ScN crystals. The EDS analysis (inset on the right-up corner) shows that YN crystals are composed mainly of yttrium and nitrogen elements. Semiquantitative analysis based on the EDS spectrum reveals the atom ratio of N:Y to be about 1:1.21 which implies a high yttrium content. However, this deviation

from 1:1 stoichiometry will not contradict the above-mentioned XRD results and the reasons will be discussed later. In addition, a small fraction of O with atom ratio about 2.8% has been detected, which can be attributed to the surface oxidation. Since YN is highly reactive in moist air, the little water vapor will cause it to corrode.

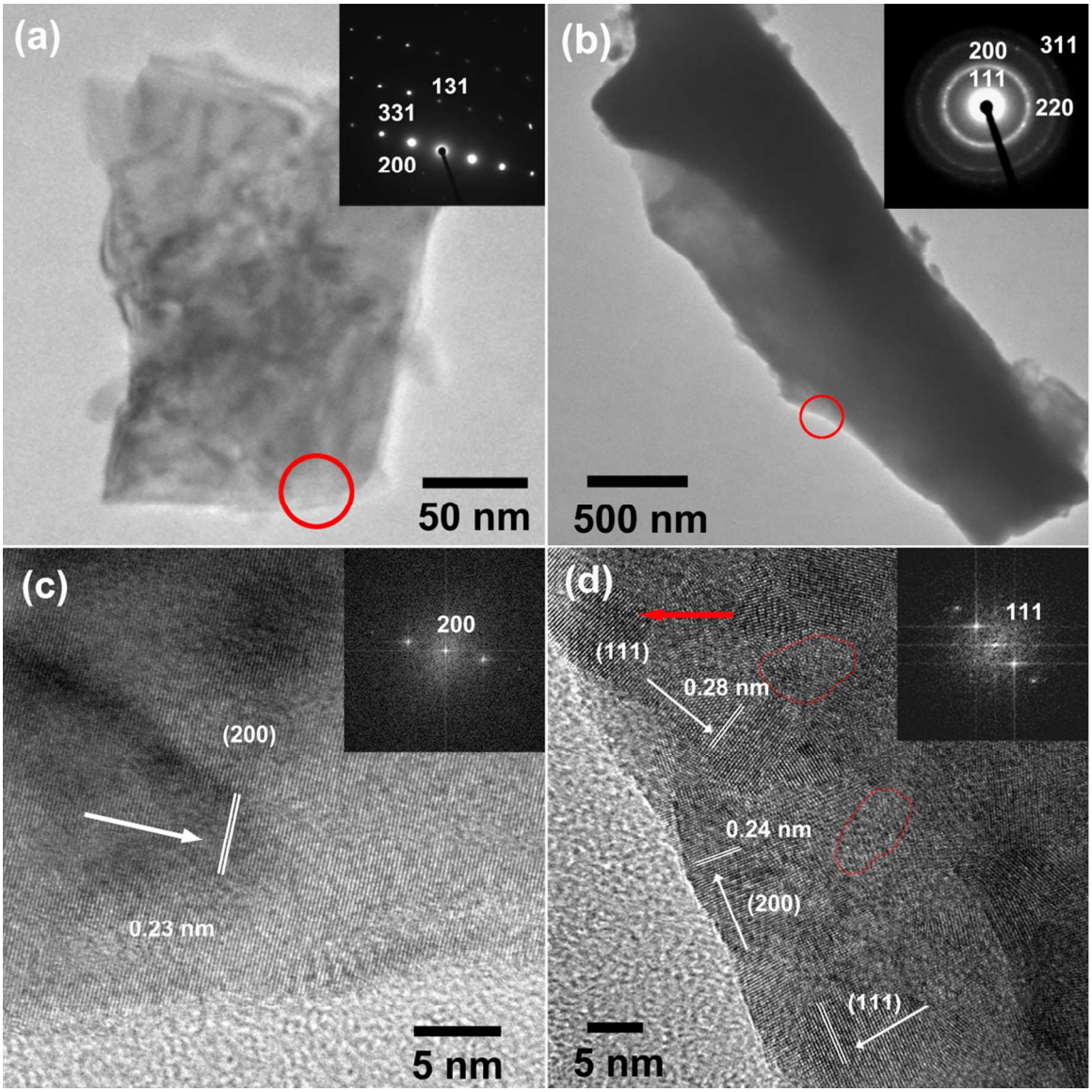

Figure 3. TEM analysis of the finely ground ScN and YN. (a), (b) are the typical images of ScN and YN fragments. The insets are the corresponding SAED patterns of the regions marked in red circles. The marked regions are also for HRTEM characterization corresponding to (c) and (d). (c) HRTEM image of ScN shows single crystalline structure with d-spacing of 0.23 nm corresponding to (200) base plane. Inset is the FFT pattern from the crystal lattice. (d) HRTEM image of YN exhibits

polycrystalline structure which is composed of small single crystals with random crystallographic orientations. Inset is the FFT pattern from the region indicated by red arrow.

For further investigate the structure of these ScN and YN crystals, the samples were ground into fine powders and characterized in further detail using TEM as shown in Figure 3. Figure 3a shows a bright-field image of the ScN fragment and the corresponding SAED pattern can be indexed to the face-centered cubic ScN lattice which is in good agreement with the XRD results (Figure 1a). Figure 3c presents the HRTEM image (recorded from red circle in Figure 3a), which shows that the ScN crystals are single crystals with clear lattice fringes. The distance between adjacent lattice planes is about 0.23 nm, and this corresponds well with the d-spacing of (200) crystal planes of face-centered cubic ScN. The inset in Figure 3b is the corresponding SAED pattern of the YN fragment marked in red circle, the four clear diffraction rings can be indexed with the (111), (200), (220), (311) crystal planes of face-centered cubic YN, in good agreement with the XRD results. According to XRD result, we think the diffraction pattern implies the polycrystalline structure of the YN crystals. Figure 3d is the HRTEM image from the region highlighted by red circles in Figure 3b, from which we can see that the YN crystals are composed of single crystal particles with clearly crystal boundaries and different crystal particles exhibit different base planes. As shown in Figure 3d, the typical d-spacing of 0.28 nm and 0.24 nm corresponding to the (111) and (200) planes of face-centered cubic YN, respectively. Inset in Figure 3d is the Fast Fourier Transform (FFT) pattern of the region marked by red arrow.

Since XRD show that ScN and YN crystals are of high crystalline quality, the off-stoichiometry of them must be explained by the existence of various point defects. Possibilities could include metal (M)-on-N-site (M_N) antisite defects or metal interstitials; however, since these could lead to local metallic bonding with different structure (i.e., Sc and Y metal are hexagonal), we would expect substantial degradation of the NaCl crystal structure, which we do not find even in the high metal content of YN. We therefore think

that a more plausible explanation is the formation of N vacancies. Investigation on the conditions of formation of rare-earth nitrides has shown that the formation of yttrium-group metals nitrides in both molecular nitrogen and ammonia the limiting value of nitrogen content is not attained (the actual content is 8-10% lower than the theoretical).[23] This is attributable to the high dissociation pressure of yttrium-group metal nitrides of limiting compositions, as a result of which these nitrides can only be produced under high nitrogen pressure.[23] However, even we provide excess nitrogen pressure the Y content in YN is still much higher than that Sc in ScN referring to the EDS results, which implies a large N vacancies concentration in YN.

Generally, NaCl-structure transition metal nitrides are known to exhibit large single phase fields, thus they can sustain large vacancy concentrations.[7] For example, TiN is stable in the NaCl structure for N/Ti ratios ranging from 0.6 to 1.2.[40] This is discussed in terms of a vacancy stabilization mechanism emphasizing the role of metal-metal interactions that form around a nitrogen vacancy.[41] Huisman *et al*[42] had shown that it is possible for vacancies to lower the total energy (increase the bond strength) of a compound due to the appearance of vacancy-induced defect states below the Femi level caused by clusters of atoms of one of the constituents. In the B1 type structure of the TMNs, removing a nitrogen atom allows the six metal atoms surrounding the vacancy to form strengthened metallic bonding while the covalent bonding is weakened.[41] In this picture the gain of energy due to the creation of metal-metal interactions compensated the loss of energy due to the suppression of nitrogen-metal covalent interactions, the final result being a lowering of the total energy and stabilization of the nitrogen deficient compound.[41] It is obvious that removing a nitrogen atom would be energetically less favorable in ScN than in YN: as the covalent bonding in ScN can be seen to be stronger than that in YN in light of the larger Y-N bond (bond length, Sc-N ~2.25 Å,[6, 43] Y-N~2.45 Å[44]) but the metallic interactions of Sc-Sc are close to and even weaker than that of Y-Y as indicated by theoretical[45, 46] and experimental[47] studies. The competitive mechanism

between nitrogen-metal interactions and metal-metal interactions in ScN and YN allows us to understand why YN form with larger nitrogen vacancies concentration than ScN. Further observation into the HRTEM image of YN (Figure 3), we find that except for the YN single crystal particles, a small fraction of amorphous domains distribute among the YN grains as indicated by red dash lines. In consideration of the XRD and EDS results of YN, we deduce the formation of non-crystalline phase of metal Y in YN and this contribute to the high contents of Y in the EDS results. As discussed above, the introduction of a nitrogen vacancy in the B1 structure of YN will create a cluster of six metallic atoms. The symmetry of the cluster is similar to the local symmetry around a metallic atom in the hexagonal closed-packed lattice of Y metal. Thus the cluster can be approximately regarded as a piece of Y metal in YN (neglecting the interactions between the cluster and the rest of the crystal).[41] However, in the DC arc plasma system the growth of products always experiences high quench rate (i.e., 10^3 K/S) as a result of the large temperature gradient,[48, 49] which would result in the disordered arrangements of the clusters of Y atoms and then forming non-crystalline structure upon quenching. Investigation on amorphous phase in Au-Si system and other amorphous alloys evidenced that non-crystalline structures can be obtained for some, perhaps all, metals and alloys by quenching rapidly enough from the molten state.[50-52]

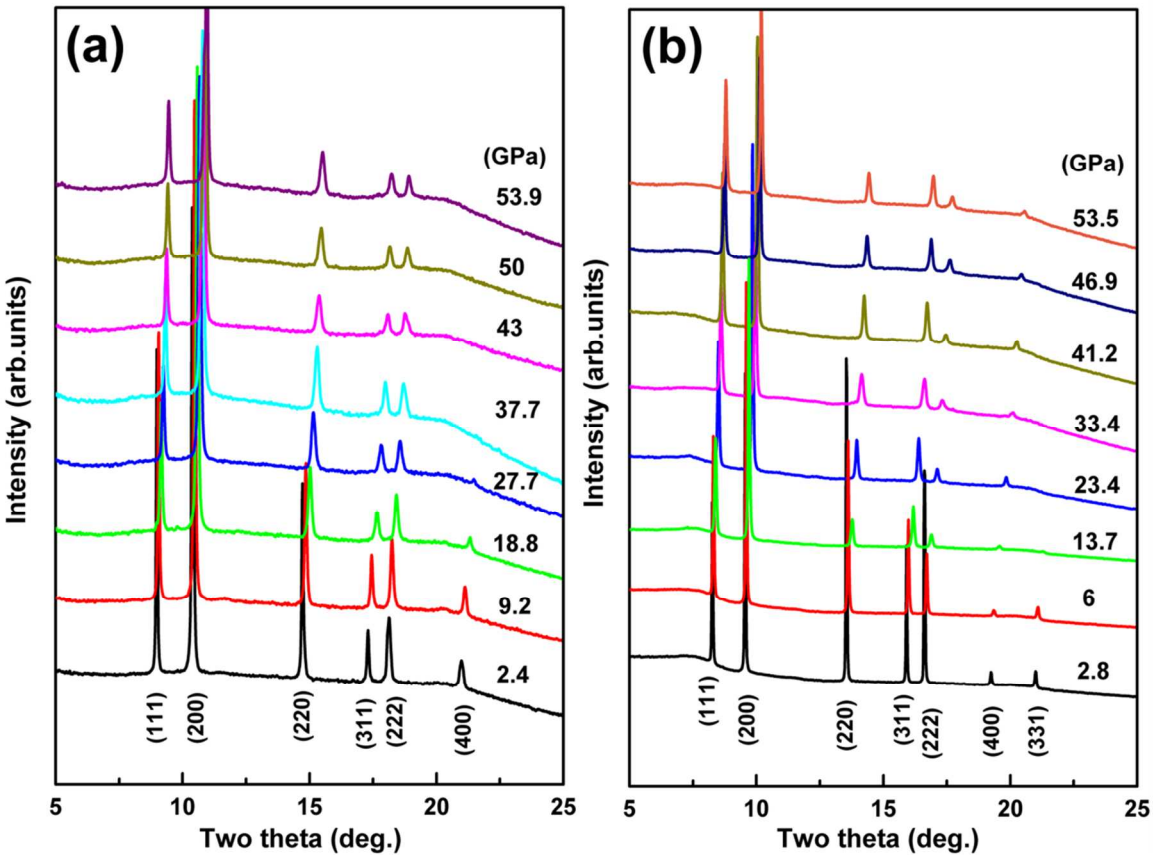

Figure 4. High pressure X-ray diffraction patterns of ScN (a) and YN (b) at different pressures. The diffraction peaks are denoted with Miller indices. No phase transition occurs during the whole compression process.

The obtained ScN and YN are investigated by in situ angle-dispersive synchrotron X-ray diffraction for the further exploration of their structural and elastic properties. Representative high-pressure XRD patterns are shown in Figure 3. The diffraction peaks are denoted with Miller indices and can be indexed to the pure rocksalt (B1) structure ScN (Figure 3a) and YN (Figure 3b). During the entire compression processes, all the peaks shift to higher angles with increasing pressure and no extra peaks appear in the XRD patterns. The Rietveld refinements of ScN and YN (Figure 4) performed at 53.9 GPa and 53.5 GPa showing good agreement with cubic crystal structure (space group Fm3m) with residuals R_{wp}=0.68% and 1.45%, respectively. Combing the high-pressure XRD and refinements results, it is suggested that there are no phase transitions in the

pressure ranges we achieved in this study. To our knowledge, this is the first time that the effects of pressure on ScN and YN have been studied experimentally. Our results are in accord with the theoretical studies that ScN and YN are stable under high pressure.[3, 31-35]

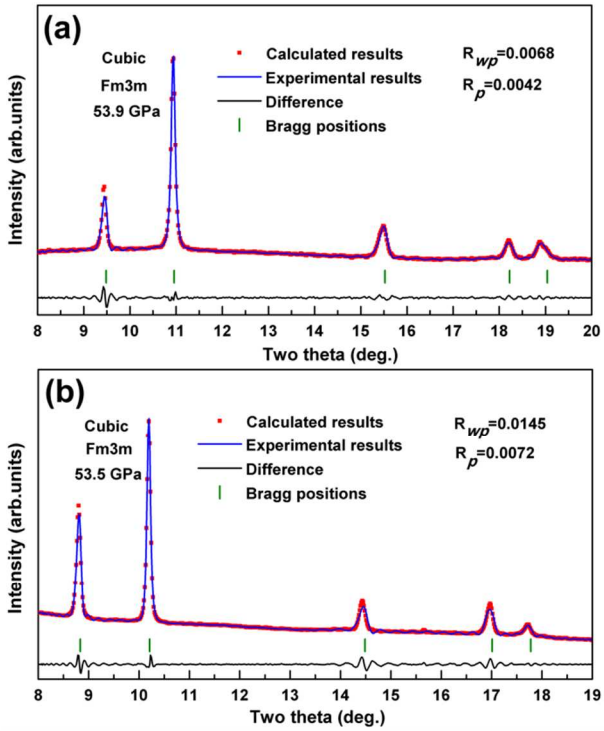

Figure 5. Rietveld refinement of the XRD patterns of ScN (a) and YN (b) taken at 53.9 and 53.5 GPa, respectively. Bars are marked at the positions of diffraction peaks.

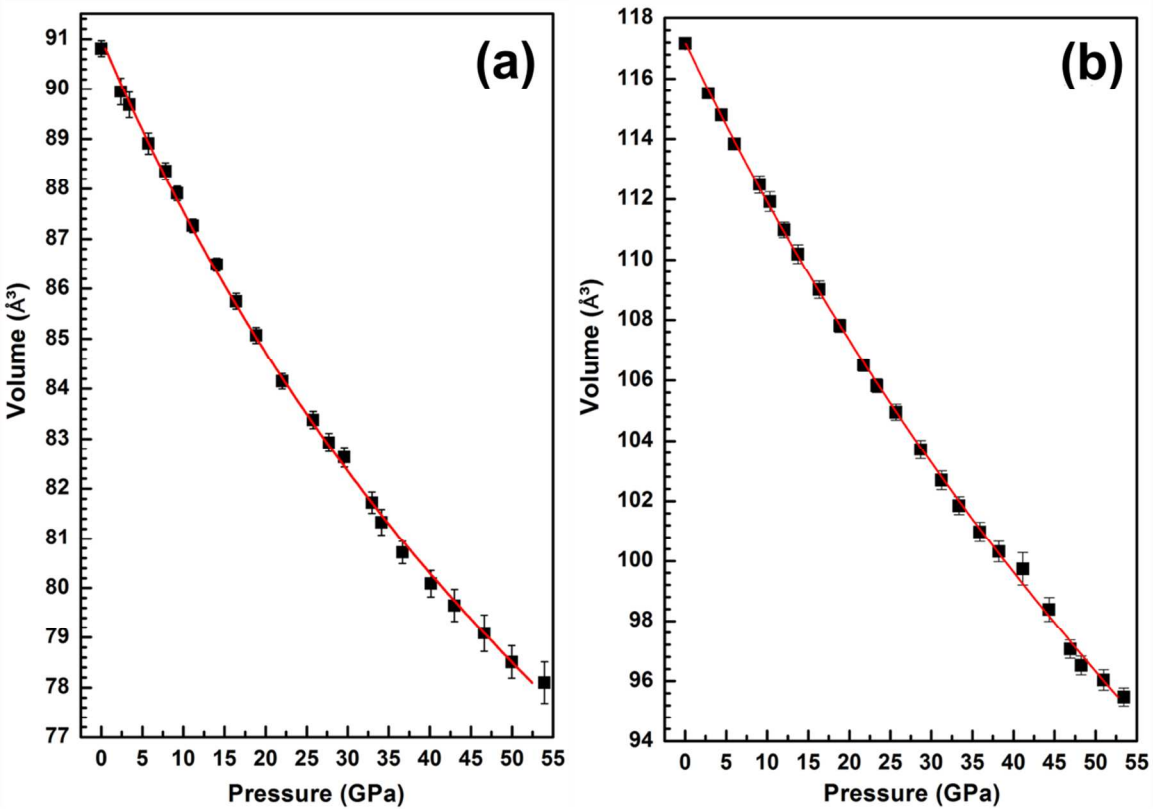

Figure 6. Pressure-volume relations of ScN (a) and YN (b). The results are fitted to a third order Birch-Murnaghan equation. The error bar is the standard deviation of mean.

Variations of volume with pressure for ScN and YN are plotted in Figure 5. Fitting the pressure-volume data to the third-order Brich-Murnaghan (BM) equation of state (EOS) yield the bulk modulus of B_0 = 221(13) GPa with B_0' = 6.8(1.7) for ScN. This result is well consistent with theoretical value 201-222 GPa[3, 6, 37, 38] and experimental value 182 ± 40 GPa.[18] The agreement between theory and experiment is very good. However, when fitting the pressure-volume data of YN to this equation, we obtain a bulk modulus of B_0 = 209(6) GPa with B_0' = 2.7(0.8) exhibiting a reduced compressibility compared to those theoretical values which spread in the range of 154-163 GPa[6, 34, 35] as listed in Table 1.

Table 1. Comparison of experimental and theoretical lattice constant *a*, bulk modulus B_0 and pressure derivative B'_0 at equilibrium volume for ScN and YN compounds

System	*Method*	*a (Å)*	B_0 *(GPa)*	B'_0
ScN	Present work (EOS)	4.498	221.082	6.813
	Present work (F_E-f_E)		223.102	7.206
	Experimental woks	4.501[a]	182±40[a]	
	Theoretical wokds	4.54[b], 4.44[c] , 4.50[d], 4.42[e], 4.455[f], 4.516[g]	201[b], 220[c], 201[d], 235[e], 221[f], 217[g],	3.31[b], 4.30[e], 4.27[f], 3.15[g],
YN	Present work (EOS)	4.894	209.055	2.726
	Present work (F_E-f_E)		204.051	2.960
	Experimental works	4.88[h]		
	Theoretical works	4.85[b], 4.93[i], 4.915[j], 4.90[k]	163[b], 157[i], 154[j], 160[k]	3.50[i],3.06[j]

[a] Ref. [18]
[b] Ref. [3] using FP-LAPW (GGA).
[c] Ref. [3] using FP-LAPW (LDA).
[d] Ref. [6] using FP-LAPW (GGA).
[e] Ref. [6] using FP-LAPW (LDA).
[f] Ref. [37] using PP-PW (LDA)
[g] Ref. [38] using GGA.
[h] Ref. [28]
[i] Ref. [34] using FP-LAPW (GGA).
[j] Ref. [35] using FP-LAPW (GGA).
[k] Ref. [44] using GGA

In order to obtain a direct indication of the compressional behavior of ScN and YN and of the quality of the EOS fit, the *P–V* data are transformed into *F–f* data where *F* is the normalized stress and *f* the finite strain. For the Birch-Murnaghan EOS, based upon the Eulerian definition of finite strain f_E, the normalized pressure is defined as $F_E = P/(3f_E(1+2f_E)^{5/2})$ with the Eulerian strain defined as $f_E = [(V_0/V)^{2/3}-1]/2$.[53] In a F_E-f_E plot, if the data points all lie on a horizontal line of constant F_E then $B_0' = 4$, and the data can be fitted with a second order BM. If the data lie on an inclined straight line, the slope is equal to $3B_0(B_0'-4)/2$, and the data will be adequately described by a third-order BM. In both cases, the intercept on the vertical F_E axis is the value of B_0. The F_E - f_E plots for ScN and YN are shown in Figure 6 with the uncertainties in f_E and F_E. It seen that linear

fits to the experimental data present two inclined lines with a positive slope for ScN and a negative one for YN. The yielding B_0' are 7.206 and 2.96 for ScN and YN, respectively. These results suggest that a third-order BM EOS is appropriate for the representation of the pressure-volume relations for ScN and YN. The differences in B_0 and B_0' obtained from EOS analysis and the linear fit of the *F(f)*-plots are listed in Table 1, the EOS fit can be considered of good quality.

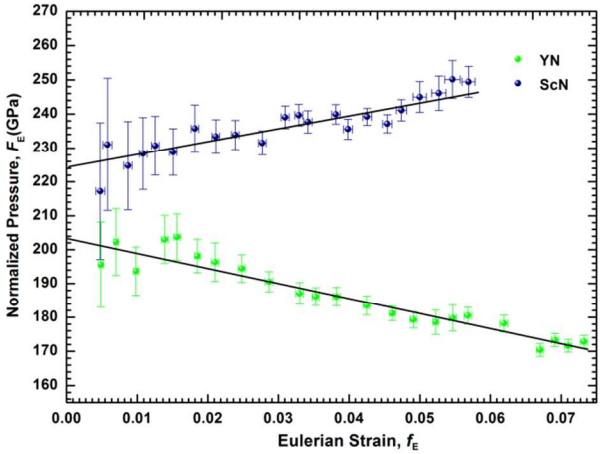

Figure 7. Volume-pressure data of ScN (a) and YN (b) displayed as a plot of the normalized pressure F_E against the Eulerian strain f_E. The linear fits to the experimental data present two inclined lines with a positive slope for ScN and a negative one for YN. The error bar is the standard deviation of mean.

As there are no experimental measurements of bulk modulus of YN for comparison, we mainly concentrate on several factors such as hydrostatic pressure, vacancy defects and grain sizes, which would affect the compressibility of YN. Systematical studies on the compressibility of nanocrystalline materials showed that the bulk modulus significantly enhanced when measured under nonhydrostatic conditions.[54, 55] As can be seen in the HRTEM image (Figure 3d), the polycrystalline structure of YN is mainly composed of small single crystals with random crystallographic orientations and dimensions ranging from 5 to 15 nm. Because of the very large number of grain boundaries in this polycrystalline YN, all with a different orientation relative to the main force direction, the applied pressure can be considered hydrostaticlike.[56] It is expected that vacancies reduce the number of chemical bonds and hence the strength of materials.

Theoretical and experimental results have shown that the elastic moduli of group IVb nitrides such as TiN_x, ZrN_x, and HfN_x decrease as the concentration of the nonmetal vacancy increases.[57] Consequently, the introduction of vacancy defects in YN would contribute negatively to the bulk modulus. In general, with the decrease in particle size in nanocrystalline materials, the bulk moduli elevate apparently as compared with their bulk materials.[58, 59] This can be explained by a higher surface energy contribution.[60] Previous studies on a significant ratio of nanocrystalline materials evidenced that the reduction of particle size can significantly lead to an enhancement of bulk modulus.[58, 61] Moreover, as nanocrystalline materials have lots of grain boundaries and fewer dislocations, according to the Hall-Petch effect,[62, 63] the hardness and yield stress of the material typically increases with decreasing grain size, which also implies an enhanced strength against compression, i.e. reduces the compressibility. Therefore, we come to the conclusion that the decreased grain size in YN should be responsible for the enhanced bulk modulus.

4. Conclusions

In summary, we synthesized ScN and YN crystals using plasma assisted DC arc discharge method. Structural characterization and EDS analysis indicate that the as-synthesized ScN crystals are stoichiometric single crystalline while YN crystals are non-stoichiometric polycrystalline with amorphous Y domains distributed among YN grains. High pressure investigations on ScN and YN show that ScN and YN are stable under very high pressure. The experimental bulk modulus for ScN coincides with those of theoretical results while YN yield a bulk modulus much higher than the theoretical values. The higher surface energy, large quantity of grain boundaries and fewer dislocations, which arising from the decreased grain sizes in the characteristic polycrystalline YN should be responsible for the improved bulk modulus. Highly structural stability as well as low compressibility makes ScN and YN potential candidates for various applications under extreme conditions.

Acknowledgements

This work was supported financially by the National Natural Science Foundation of China (Grant Nos. 11074089, 51172087, 11304111, NSAF. No: U1330115), Specialized Research Fund for the Doctoral Program of Higher Education of China (20110061110011) and the National Basic Research Program of China (Grant No. 2011CB808204).

References

1 D. Holec, M. Friak, J. Neugebauer and P. H. Mayrhofer, *Phys. Rev. B*, 2012, **85**, 064101.
2 P. V. Burmistrova, J. Maassen, T. Favaloro, B. Saha, S. Salamat, Y. Rui Koh, M. S. Lundstrom, A. Shakouri and T. D. Sands, *J. Appl. Phys.* , 2013, **113**, 153704.
3 N. Takeuchi, *Phys. Rev. B*, 2002, **65**, 045204.
4 J. M. Gregoire, S. D. Kirby, G. E. Scopelianos, F. H. Lee and R. B. van Dover, *J. Appl. Phys.* , 2008, **104**, 074913.
5 H. A. Al-Brithen, A. R. Smith and D. Gall, *Phys. Rev. B*, 2004, **70**, 045303.
6 C. Stampfl, W. Mannstadt, R. Asahi and A. Freeman, *Phys. Rev. B*, 2001, **63**, 155106.
7 A. R. Smith, H. A. H. Al-Brithen, D. C. Ingram and D. Gall, *J. Appl. Phys.* , 2001, **90**, 1809.
8 M. E. Little and M. E. Kordesch, *Appl. Phys. Lett.* , 2001, **78**, 2891.
9 F. Perjeru, X. Bai, M. I. Ortiz-Libreros, R. Higgins and M. E. Kordesch, *Appl. Surf. Sci.* , 2001, **175-176**, 490-494.
10 J. P. Dismukes and T. D. Moustakas, *Proc. Electrochem. Soc.*, 1996, **96-11**, 111.
11 K. Shimada, A. Zenpuku, K. Fujiwara, K. Hazu, S. F. Chichibu, M. Hata, H. Sazawa, T. Takada and T. Sota, *J. Appl. Phys.* , 2011, **110**, 074114.
12 D. Gall, I. Petrov and J. E. Greene, *J. Appl. Phys.* , 2001, **89**, 401.
13 J. M. Gregoire, S. D. Kirby, M. E. Turk and R. B. van Dover, *Thin Solid Films* 2009, **517**, 1607-1609.
14 B. Saha, J. Acharya, T. D. Sands and U. V. Waghmare, *J. Appl. Phys.* , 2010, **107**, 033715.
15 B. Saha, T. D. Sands and U. V. Waghmare, *J. Phys.: Condens. Matter* 2012, **24**, 415303.
16 X. Jia, W. Yang and M. Qin, *Appl. Phys. Lett.* , 2008, **93**, 222501.
17 A. Herwadkar and W. Lambrecht, *Phys. Rev. B*, 2005, **72**.
18 D. Gall, I. Petrov, N. Hellgren, L. Hultman, J. E. Sundgren and J. E. Greene, *J. Appl. Phys.* , 1998, **84**, 6034.
19 X. W. Bai and M. E. Kordesch, *Appl. Surf. Sci.* , 2001, **175-176**, 499-504.
20 M. A. Moram, S. V. Novikov, A. J. Kent, C. Nörenberg, C. T. Foxon and C. J. Humphreys, *J. Cryst. Growth* 2008, **310**, 2746-2750.
21 W. Lengauer, *J. Solid State Chem.* , 1988, **76**, 415.
22 P. K. Charles, N. H. Krikorian and C. M. Joseph, *J.Phys.Chem.*, 1957, **61**, 1237.
23 M. D. Lyutaya and A. B. Goncharuk, *Powder Metall. Met. Ceram.* , 1979, **18**, 569-574.
24 M. D. Lyutaya, A. B. Goncharuk and I. I. Timofeeva, *Tranl. Zh. Prikl. Khim.*, 1975, **48(4)**, 721-724.
25 G. V. Samsonov, M. D. Lyutaya and V. S. Neshpor, *Zh. Prikl. Khim.* , 1962, **36**, 2108.
26 R. Niewa, D. A. Zherebtsov, M. Kirchner, M. Schmidt and W. Schnelle, *Chem. Mater.* , 2004, **16**, 5445-5451.

27 Z. Gu, J. H. Edgar, J. Pomeroy, M. Kuball and D. W. Coffey, *J. Mater. Sci. - Mater. Electron.* , 2004, **15**, 555-559.

28 L. Du, J. H. Edgar, R. A. Peascoe-Meisner, Y. Gong, S. Bakalova and M. Kuball, *J. Cryst. Growth* 2010, **312**, 2896-2903.

29 J. V. Badding, *Annu. Rev. Mater. Sci.* , 1998, **28**, 631-658.

30 A. Mujica, A. Rubio, A. Muñoz and R. Needs, *Rev. Mod. Phys.* , 2003, **75**, 863-912.

31 A. Tebboune, D. Rached, A. Benzair, N. Sekkal and A. H. Belbachir, *Phys. Status Solidi B* 2006, **243**, 2788-2795.

32 A. Maachou, B. Amrani and M. Driz, *Physica B* 2007, **388**, 384-389.

33 W. X. Feng, S. X. Cui, H. Q. Hu, G. Q. Zhang, Z. T. Lv and Z. Z. Gong, *Physica B* 2010, **405**, 2599-2603.

34 L. Mancera, J. A. Rodriguez and N. Takeuchi, *J. Phys.: Condens. Matter* 2003, **15**, 2625-2633.

35 B. Amrani and F. El Haj Hassan, *Comput. Mater. Sci.* , 2007, **39**, 563-568.

36 H. Berkok, A. Tebboune and M. N. Belkaid, *Physica B* 2011, **406**, 3836-3840.

37 A. Qteish, P. Rinke, M. Scheffler and J. Neugebauer, *Phys. Rev. B*, 2006, **74**, 245208.

38 M. G. Brik and C. G. Ma, *Comput. Mater. Sci.* , 2012, **51**, 380-388.

39 W. W. Lei, D. Liu, Y. M. Ma, X. H. Chen, F. B. Tian, P. W. Zhu, Q. L. Cui and G. Z. Zou, *Angew. Chem. Int. Ed.* , 2010, **49**, 173-176.

40 B. O. J. J.-E. Sundgren, A. Rockett, S. A. Barnett, and J. E. Greene, J., *Physics and Chemistry of Protective Coatings,* edited by J. E. Greene, W. D. Sproul, and J. A. Thornton*, American Institute of Physics Series Vol. 149 (AIP, New York, 1986), p. 149.*

41 L. Porte, *J. Phys. C: Solid State Phys.* , 1985, **18**, 6701-6709.

42 L. M. Huisman, A. E. Carlsson, C. D. Gelatt and H. Ehrenreich, *Phys. Rev. B*, 1980, **22**, 991-1006.

43 D. Gall, I. Petrov, L. D. Madsen, J.-E. Sundgren and J. E. Greene, *J. Vac. Sci. Technol. A*, 1998, **16**, 2411.

44 B. Saha, T. D. Sands and U. V. Waghmare, *J. Appl. Phys.* , 2011, **109**, 073720.

45 L. Schimka, R. Gaudoin, J. Klimes, M. Marsman and G. Kresse, *Phys. Rev. B*, 2013, **87**, 214102.

46 P. Janthon, S. M. Kozlov, F. Viñes, J. Limtrakul and F. Illas, *J. Chem. Theory Comput.* , 2013, **9**, 1631-1640.

47 D. A. Young, *Phase Diagrams of the Elements, University of California Press: Berkeley, CA*, 1991, 273-381.

48 K. C. Hsu, K. Etemadi and E. Pfender, *J. Appl. Phys.* , 1983, **54**, 1293.

49 S. M. Aithal, V. V. Subramaniam, J. Pagan and R. W. Richardson, *J. Appl. Phys.* , 1998, **84**, 3506.

50 W. Klement, Willens, R. H. and Duwez, P., *Nature*, 1960, **187**, 869.

51 J. F. Löffler, *Intermetallics*, 2003, **11**, 529-540.

52 W. H. Wang, C. Dong and C. H. Shek, *Mater. Sci. Eng., R* 2004, **44**, 45-89.

53 R. J. Angel, *Equations of state, in: R.M. Hazen, R.T. Downs (Eds.), High-Pressure and High-Temperature Crystal Chemistry, 41, MSA Reviews in Mineralogy and Geochemistry, 2000, pp. 35–60.*

54 C. D. Grant, J. C. Crowhurst, T. Arsenlis, E. M. Bringa, Y. M. Wang, J. A. Hawreliak, P. J. Pauzauskie and S. M. Clark, *J. Appl. Phys.* , 2009, **105**, 084311.

55 B. Chen, D. Penwell and M. B. Kruger, *Solid State Commun.* , 2000, **115**, 191-194.
56 S. Trapp, C. Limbach, U. Gonser, S. Campbell and H. Gleiter, *Phys. Rev. Lett.* , 1995, **75**, 3760-3763.
57 S. H. Jhi, S. G. Louie, M. L. Cohen and J. Ihm, *Phys. Rev. Lett.* , 2001, **86**, 3348-3351.
58 Z. W. Wang, S. K. Saxena, V. Pischedda, H. P. Liermann and C. S. Zha, *Phys. Rev. B*, 2001, **64**, 012102.
59 R. D. Cong, H. Y. Zhu, X. X. Wu, C. L. Ma, G. C. Yin, X. J. Xie and Q. L. Cui, *J. Phys. Chem. C* 2013, **117**, 4304-4308.
60 J. Z. Jiang, J. S. Olsen, L. Gerward and S. Morup, *Europhys. Lett.* , 1999, **45**, 275.
61 Z. W. Wang, Y. S. Zhao, D. Schiferl, J. Qian, R. T. Downs, H. K. Mao and T. Sekine, *J. Phys. Chem. B* 2003, **107**, 14151.
62 E. O. Hall, *Proc. Phys. Soc., Lond. B*, 1951, **64**, 747-753.
63 N. J. Petch, *J. Iron Steel Inst.* , 1953, **174**, 25-28.

A table of contents entry.

Colour graphic:

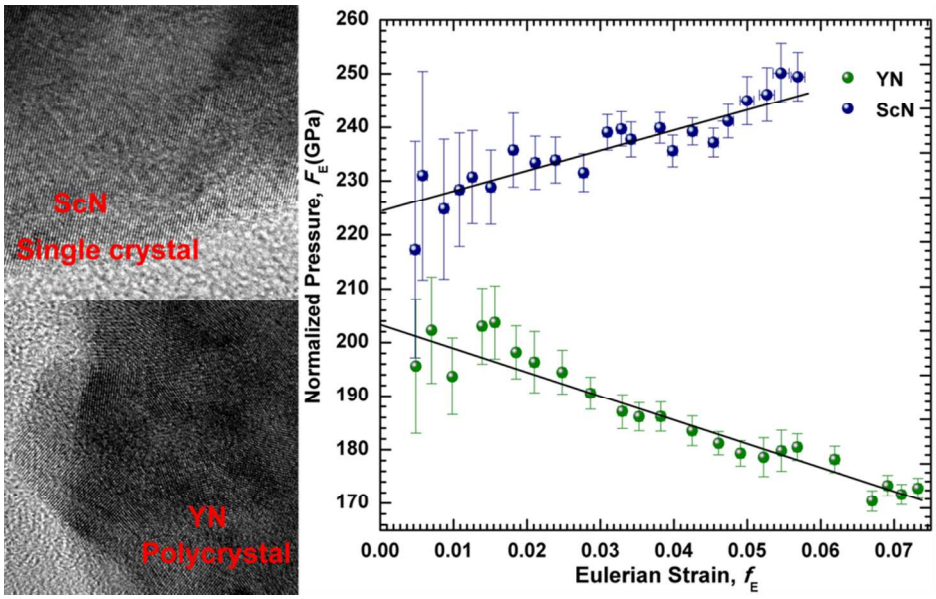

Text:

This paper investigated the arc discharge synthesis of ScN and YN and the high pressure behaviors of the samples.